

DOI: 10.1002/ ((please add manuscript number))

**Article type:** Full Paper

**Title:** Carbon Quantum Dots co-Doped with Nitrogen and Lanthanides for Multimodal Imaging

*Author(s), and Corresponding Author(s)\*:* *Diego Bouzas-Ramos, Jesus Cigales Canga, Juan Carlos Mayo\*, Rosa Maria Sainz, Jorge Ruiz Encinar, Jose M. Costa-Fernandez\**.

Dr. D. Bouzas-Ramos, J. Cigales Canga, Dr. J. Ruiz Encinar, Prof. J. M. Costa-Fernandez

Department of Physical and Analytical Chemistry, University of Oviedo, Julián Clavería 8,  
33006, Oviedo, Spain

E-mail: [jcostafe@uniovi.es](mailto:jcostafe@uniovi.es)

Dr. J. C. Mayo, Dr. R. M. Sainz

Departamento de Morfología y Biología Celular, BIOX Unit, Instituto Universitario de  
Oncología del Principado de Asturias (IUOPA), Universidad de Oviedo, 33006 Oviedo,  
Asturias, Spain

E-mail: [mayojuan@uniovi.es](mailto:mayojuan@uniovi.es)

**Keywords:** doped nanoparticles, carbon quantum dots, multimodal imaging, *in vitro* imaging,  
*in vivo* imaging

## Abstract

Nanoparticles are increasingly being used as advantageous alternatives to commonly used contrast agents in bioimaging, not only due to their improved imaging capabilities but also because their great potential in theranostics. Herein, carbon Quantum Dots (CQDs) co-doped with nitrogen and lanthanides (i.e. Gd and Yb) are synthesized using an one-pot microwave-assisted hydrothermal method and evaluated as improved multimodal contrast agents for imaging purposes. Obtained doped-CQDs exhibit an intense fluorescence emission with excellent quantum yields ( $66 \pm 7\%$ ) along with outstanding magnetic resonance (MR) and computed tomography (CT) contrast properties, without showing appreciable cytotoxicity after their exposure to three different cell lines for 24 h and 72 h. Such outstanding features turn these nanoparticles into ideal labels for multimodal imaging. To actually prove such potential, firstly, these CQDs co-doped with N and lanthanides are successfully applied to *in vitro* fluorescence, MR and CT cell imaging. In addition, such nanoparticles demonstrate to have a great potential as contrast agents for multimodal imaging *in vivo* as significant MR and CT contrast-enhancement is observed in the bladder and kidneys of a mouse after their intravenous injection into the tail vein.

## 1. Introduction

Advances in biotechnology and medicine have promoted the development of novel nanoparticles (NPs) for their use in bioimaging, as they offer several important advantages as imaging contrast agents over conventional molecular-scale compounds, including: high loading capacity, where the concentration of imaging agents in the NP can be controlled during the synthesis, easy NP surface functionalization for nanoprobe development and multimodal imaging capabilities.<sup>[1,2]</sup> Particularly, NPs have recently emerged as excellent contrast agents in multimodal imaging, a cutting-edge technology that allows to obtain complementary and integrated information highly valuable nowadays in clinical diagnosis.

Additionally, NPs have great potential to be used not only for imaging but also simultaneously in targeted therapy.<sup>[1]</sup>

Up to date, NPs have been exploited as contrast agents in different imaging modalities, being fluorescence one of the most successfully exploited. Fluorescence imaging has the capacity for single cell sensitivity but has limited spatial resolution and does not provide morphological information.<sup>[2]</sup> Widely used magnetic resonance imaging (MRI) is a powerful alternative in clinical studies due to its high special resolution and depth of penetration into the tissues, providing anatomical details and information about soft tissues and organs.<sup>[2,3]</sup> Other routinely used technique is computed tomography (CT) imaging, which provides information about structure and is most sensitive to electron-dense elements (such as those found in bones). CT has several strengths such as high spatial resolution and excellent quantitative capabilities. However, the technique also present some drawbacks including a limited level of accuracy when use for screening of some diseases due to the poor sensitivity.<sup>[3,4]</sup> Separately each imaging technique exhibits different strengths in terms of resolution, sensitivity or information provided, but they have also several important drawbacks limiting their use in diagnosis. Interestingly, the synergic combination of these different clinical imaging modalities on the same nanoprobe would join strengths and compensate weaknesses facilitating and improving diagnosis or therapy.<sup>[1-5]</sup>

In this context, progress in nanotechnology enabled the development of multifunctional NPs that integrate two or more imaging contrast agents allowing their simultaneous detection by different imaging techniques. Most reported examples of these types of multifunctional nanomaterials consist of multicomponent platforms such as NaYbF<sub>4</sub>:Tm<sup>3+</sup>/NaGdF<sub>4</sub> core/shell nanocrystals,<sup>[6]</sup> Gd<sup>3+</sup> complex-modified NaLuF<sub>4</sub>-based upconversion nanophosphors,<sup>[7]</sup> GdOF:Ln@SiO<sub>2</sub>-ZnPc-CDs mesoporous capsules<sup>[8]</sup> and MnSiO<sub>3</sub>-coated upconversion NPs@g-C<sub>3</sub>N<sub>4</sub> quantum dots (QDs),<sup>[9]</sup> among others. Such described multifunctional structures exhibit very interesting properties for imaging purposes. However, some of them suffer of a

limited stability in biological media and synthetic procedure is somehow complex. Undeniably, to be routinely used in clinical diagnosis, a multimodal nanoprobe should join high imaging contrast efficiencies with good stability in biological media and low cytotoxicity. Importantly, NPs acting as imaging nanoprobes should also be easily surface functionalized with appropriate biomolecules to provide them with specificity as well.

During last years, carbon-based NPs (commonly called Carbon Dots) has witnessed a rapid development.<sup>[10-12]</sup> Depending on its properties and characteristics, carbon-based NPs can be found reported as Graphene Quantum Dots (GQDs), Carbon Quantum Dots (CQDs) or Carbon NanoDots (CNDs).<sup>[12]</sup> In all the cases, those carbon-based nanomaterials have demonstrated many of the strengths above-mentioned such as high luminescence, biocompatibility, good stability, low cytotoxicity, low-cost synthetic preparation and easy functionalization.<sup>[10,11]</sup> Additionally, synthetic procedures are many often quite simple, directly in water media and employing natural organic compounds as precursors. For those reasons, they are considered nowadays as versatile nanostructures with high potential to be used in a broad range of applications, including fluorescence bioimaging,<sup>[13]</sup> multicolor patterning and sensors,<sup>[14]</sup> and, even, MR imaging after their doping with Gd<sup>[15-16]</sup> or with Mn<sup>[17]</sup> ions. Nonetheless, to the best of our knowledge, Carbon Dots exhibiting multifunctional capabilities for multimodal bioimaging, including simultaneous fluorescence, MRI and CT imaging contrast capabilities in the same single carbon-based nanoprobe, has been never reported yet.

In the present study, we propose a facile and efficient synthetic approach to obtain Carbon Quantum Dots co-doped with N, Gd and Yb thus resulting in a single multimodal contrast agent for *in vitro* and *in vivo* multimodal imaging. For this purpose, citric acid (carbon precursor) and inorganic salts of Gd<sup>3+</sup> and Yb<sup>3+</sup> (doping ions) were used for the synthesis of these co-doped CQDs *via* a facile and low-cost one-pot microwave-assisted hydrothermal method. The herein synthesized co-doped CQDs exhibited intense and stable fluorescence

emission, with excellent quantum yield, and good MR and CT contrast capabilities. Such CQDs co-doped with N, Gd and Yb were successfully evaluated as contrast agents for *in vitro* fluorescence cell imaging and for both *in vitro* and *in vivo* MRI and CT imaging.

## 2. Results and discussion

Carbon Quantum Dots co-Doped with Nitrogen and Lanthanides were synthesized employing citric acid, ethylenediamine and both lanthanide salts as precursors, following a one-pot microwave-assisted hydrothermal route (the optimized synthetic procedure is described in the Experimental section). During the procedure, carried out at high temperature in aqueous media, carbon precursor and passivation agents were subjected to carbonization and passivation processes in order to generate carbon nuclei (CQDs).<sup>[11]</sup> In addition, the lanthanide ions were coordinated and combined with the CQDs during the formation of the carbon NPs, to get the co-doped CQDs. Resulting NPs were subsequently purified by dialysis before their exhaustive characterization and application for imaging purposes.

Figure 1a shows the high resolution-transmission electron microscopy (HR-TEM) image of a purified sample resulting from the synthesis of the doped CQDs, confirming the formation of quasi-spherical CQDs with low polydispersity. The nanoparticle average size and the size distribution of the synthesized co-doped CQDs were estimated after HR-TEM image processing, using the ImageJ software (public domain Java image processing program). A fairly uniform nanoparticle average size of 3.5 nm was obtained, with NPs diameter distributed in the range from 2.2 to 4.8 nm (n=100 individual NPs), (see Figure 1b). Furthermore, energy dispersive X-ray spectroscopy (EDX) allowed us to corroborate that both lanthanide ions were incorporated in the final nanostructures. Figure 1c shows the EDX analysis of the co-doped CQDs, confirming the successful incorporation of Gd and Yb in the CQDs.

The X-ray powder diffraction (XRD) pattern of the co-doped CQDs synthesized (Supporting Information Figure S1) displayed a broad diffraction peak centered at 23.5° ( $d$ -spacing=0.38 nm), which is in accordance with the typical XRD pattern of undoped CQDs.<sup>[14]</sup> This broad peak suggested a carbon material with some graphitic sp<sup>2</sup> carbon atoms, since the peak of the pattern was attributed to the (002) reflection of the graphite structure.

Fourier transform-infrared spectroscopy (FT-IR) was used to identify the functional groups present on the surface of the CQDs thus providing water stability to the NPs. FT-IR spectrum of co-doped CQDs was collected in the range between 800 and 3800 cm<sup>-1</sup> (Supporting Information Figure S2), and the following absorption bands were observed: the broad band between 3000 – 3500 cm<sup>-1</sup> is identified to the stretching vibration of O-H and N-H; the small band at 2935 cm<sup>-1</sup> is assigned to C-H bond; the band centered at 1650 cm<sup>-1</sup> is attributed to the stretching vibration of C=O and C=C; peaks between 1475 and 1250 cm<sup>-1</sup> could be ascribed to C-N and N-H groups; and the peak at 1030 cm<sup>-1</sup> could be corresponded to stretching modes of C-O-C and C-O functional groups.<sup>[14]</sup> In brief, the FT-IR analysis revealed the coexistence of different types of functional groups on the surface of the synthesized CQDs, in which the oxygen-containing functional groups on their surface enable a better stabilization of these carbon-based NPs in water.

In order to demonstrate the usefulness of the obtained nanoparticles as eventual tags for optical bioimaging applications, the optical properties of the co-doped CQDs suspended in aqueous solution were assessed by UV-vis spectrophotometry and fluorescence spectroscopy. UV-vis absorption and fluorescence spectra of a sample containing the CQDs in aqueous media are shown in **Figure 2a**. Interestingly, the UV-vis spectrum exhibited two absorption peaks at 245 and 350 nm. Accordingly to bibliography,<sup>[18]</sup> they can be ascribed to  $\pi\rightarrow\pi^*$  transition of the C=C bond and to  $\eta\rightarrow\pi^*$  transition of the C=O bond (which can be evidence of the presence of carboxyl functional groups on the surface of the co-doped CQDs), respectively.

On the other hand, synthesized CQDs displayed a strong blue fluorescent emission centered at 440 nm when excited with a 350 nm UV radiation (as it is shown in **Figure 2a**). Doping the CQDs with Gd and Yb does not alter the original photoluminescence properties of the undoped NPs (see Supporting Information Figure S3).

**Figure 2b** shows the emission signal from the CQDs under continuous illumination. Noticeably, the carbon-based nanoparticles here synthesized exhibited a strong fluorescence emission in the presence of dissolved oxygen that is changeless when the NPs are introduced in high ionic strength environments (e.g. biological media). Moreover, such luminescence emission remains unaltered even being exposed to a high energy 350 nm UV lamp during 120 min, being a proof of the high photostability of the nanoparticles. The pH of the media causes only a slight effect on the emission of the CQDs, it should be noticed that higher values of the fluorescence intensities are obtained at basic pHs.

Fluorescence lifetimes and quantum yield (QY) of the fluorescent NPs were determined. The fluorescence decay curve of the co-doped CQDs fitted well to an exponential function, which showed a tri-exponential behavior (see Figure S4 in the Supporting Information). Specifically, the longest decay time of the co-doped CQDs was  $16.0 \pm 0.2$  ns, the intermediate lifetime component was  $6.2 \pm 0.4$  ns and the shortest decay time was  $1.0 \pm 0.2$  ns. It is important to note that the presence of several lifetime ranges found after analysis of the fluorescence decay time curve of the synthesized carbon nanoparticles has also been already previously reported by other authors.<sup>[19]</sup> The fluorescent quantum yield of the CQDs was calculated by using the comparative William's method and turned out to be  $66 \pm 7\%$ . Such high quantum yield value confirms that the synthesized CQDs are highly fluorescent and with a high potential for optical bioimaging purposes. Finally, it is important to note that the co-doped CQDs showed long-term stability (more than six months) when stored in aqueous solution at room temperature without any perceptible precipitation nor detectable changes in the optical characteristics.

In order to assess their potential use as probes in biomedical applications, cytotoxicity of these co-doped CQDs was evaluated in different cell types widely used as cell culture models for different physiological and pathological purposes.<sup>[20-22]</sup> For such purpose, MTT assays were carried out in three different and well-established cell lines: a recognized tumor cell line human, the cervical carcinoma HeLa cells, and two normal cell lines, mouse embryonic fibroblast NIH-3T3 cells and Chinese hamster ovary (CHO) cells. Cell viabilities were investigated after exposure of the three different cell lines to different concentrations of co-doped CQDs (0, 0.2, 2, 20, 200 and 2000 µg mL<sup>-1</sup>) for 24 h and 72 h.

Results obtained are shown in **Figure 3**. Cell viability was not affected (values above 80 %) after 24 h for every cell line and CQDs concentration assayed. For longer times of incubation, i.e. 72 h, toxicity of these co-doped CQDs towards HeLa cells (Figure 3a) was negligible for all the concentrations assayed. In the case of NIH-3T3 and CHO cells (Figure 3b and 3c, respectively), viability was for all the concentrations assayed except for the CQDs concentration of 2 mg mL<sup>-1</sup>, in which it was slightly below 80 %. Summarizing, results obtained seems to suggest that the presence of CQDs in the cell culture media does not affect significantly cell viability and proliferation for any of the cell lines assayed.

Feasibility of the fluorescent detection of the CQDs co-doped with N, Gd and Yb in cell imaging experiments was investigated as well. For this purpose, confocal fluorescence microscopy was used to visualize the distribution and the cellular uptake of the co-doped CQDs in the different cells lines used for the cytotoxicity studies (*i.e.* HeLa, NIH-3T3 and CHO cells). For cell imaging, each cell line was incubated with co-doped CQDs at a concentration of 200 µg mL<sup>-1</sup> for 24 h. After incubation, light and confocal fluorescence images of HeLa, NIH-3T3 and CHO cells (Figures 3d-f, 3g-i and 3j-l, respectively) were obtained, first under bright field illumination and further acquired using an excitation wavelength of 405 nm. Strong blue fluorescence emission was observed inside the cells treated with the co-doped CQDs, thus certifying a significant NP cell uptake and allowing the

visualization of the nanoparticle distribution within cells. In this context, co-doped CQDs were mainly found in the cytosol of either HeLa, NIH-3T3 or CHO cells (Figures 3f, 3i and 3l, respectively). Moreover, according to the microscopic observation, co-doped NPs do not enter into the nucleus after 24 h of incubation, remaining mainly in the perinuclear regions, overlapping with the Golgi/TGN/endosome region. Therefore, it can be suggested that the here synthesized NPs internalized inside the cells *via* endocytosis, similarly to the behavior of other CQDs already reported.<sup>[13]</sup> Nevertheless, other mechanisms could not be ruled out and should be further studied. Studies focused on the specific mechanisms involved in uptake<sup>[22]</sup> could provide additional data crucial for assessing the real potential of the CQDs reported here. Interestingly, maintenance of NP fluorescence emission after their internalization into cells rules out the possibility of any eventual degradation by lysosomal/autophagosome action, which demonstrates the NP stability and robustness.

Co-doping of the fluorescent CQDs with different transition elements allow also their use as improved contrast agents in magnetic resonance imaging (MRI) and computed tomography (CT) imaging. It is well-known that Gd<sup>3+</sup> ions possess several properties (such as long electronic relaxation times and half-filled f-orbital, among others) which make its complexes with different chelates highly suitable as T<sub>1</sub> MRI contrast agents. In fact, Gd-based complexes and chelates have been widely used as MR contrast agents in radiologic practice and medicine.<sup>[23]</sup> For that reason, doping CQDs with Gd<sup>3+</sup> could provide them with MR contrast capability. To evaluate it, longitudinal relaxation time (T<sub>1</sub>), transverse relaxation time (T<sub>2</sub>) and both relaxivity values (r<sub>1</sub> and r<sub>2</sub>) were measured with a 7-T MRI system. The T<sub>1</sub>-weighted MR images shown in **Figure 4a** proved that CQDs induced a positive contrast enhancement, which became higher as the concentration of Gd increased. On the other hand, intensity of brightness of the T<sub>2</sub>-weighted MR images shown in Figure 4b gradually decreased with increasing the concentration of Gd.

Thus, this paper describes a simple method to produce a single type of NP that behaves as dual ( $T_1$  and  $T_2$ ) MRI contrast agent. This is very attractive because combining simultaneously  $T_1$  and  $T_2$  contrast effects together in a single contrast agent is a breakthrough that would enable a more versatile (i.e. offering contrast in both dark and bright tissue and organs) and accurate (i.e. offering better differentiation of normal and diseased areas) MRI.

The relaxivity values ( $r_1$  and  $r_2$ ) were calculated from the slopes of linear regression fits of the relaxivity plots shown in Figure 4c (i.e. slopes of the curves in which the longitudinal ( $1/T_1$ ) and transverse ( $1/T_2$ ) relaxation rates, respectively, were plotted with respect to different Gd concentrations). The obtained  $r_1$  and  $r_2$  values were  $5.02 \text{ mM}^{-1}\text{s}^{-1}$  and  $14.45 \text{ mM}^{-1}\text{s}^{-1}$ , respectively, providing a  $r_2/r_1$  ratio of 2.88, which indicates that these co-doped CQDs are excellent species to be efficiently used as positive  $T_1$  MRI contrast agents.<sup>[24]</sup> Interestingly, it is noteworthy that the longitudinal relaxivity value ( $r_1$ ) obtained for the co-doped CQDs was greater than that reported for the commercially available Gd-DTPA contrast agent, marketed as *Magnevist*,<sup>[25]</sup> which was the first Gd-based MR contrast agent with a widespread use in clinical applications. Moreover, enormous attention has been recently paid to development of multifunctional nanoprobes with MRI contrast agents. Typical longitudinal relaxivity  $r_1$  values of these nanoparticles are in the order of the doped-CQDs here synthesized.<sup>[26]</sup>

Interestingly, research on development of novel contrast agents for biomedical imaging has recently undergone an uptick because of interest in the pursuit of new types of species and alternatives for  $\text{Gd}^{3+}$  complexes and chelates which provide multimodal capabilities or allow an efficient and selective targeting.<sup>[27]</sup> In this context, additional incorporation of  $\text{Yb}^{3+}$  as doping ion in the CQDs was studied to produce supplementary CT contrast capabilities since  $\text{Yb}$  has a high atomic number and shows high degree of X-ray absorption.<sup>[28]</sup> As a matter of fact, upconverting mesoporous capsules containing Gd and doped with lanthanides ( $\text{Yb}^{3+}$  and  $\text{Er}^{3+}$ ) have already been reported as high performance contrast agents.<sup>[7]</sup> Taking into account these considerations, the incorporation of  $\text{Yb}$  on the CQDs already doped with N and Gd to

expand the multimodal imaging capabilities of such NPs to CT was evaluated. It is noteworthy that  $\text{Yb}^{3+}$  was simultaneously added with  $\text{Gd}^{3+}$  during the simple approach performed herein to prepare such multimodal CQDs. The successful incorporation of  $\text{Gd}^{3+}$  and  $\text{Yb}^{3+}$  to the CQDs was previously proved by EDX (Figure 1c) and ICP-MS analysis.

**Figure 5a** shows that CQDs co-doped with N, Gd and Yb provides a nanomaterial exhibiting significant CT contrast. As shown in Figures 5b-c, CT values (called Hounsfield units, HU) increased linearly with increasing the concentration of Yb. Both CT phantom and color-mapped images (Figure 5b) showed the positive contrast enhancement produced by the co-doped CQDs as the concentration of both doping ions increased. Moreover, the slope of the linear relationship between CT values versus different concentrations of Yb (14.4 HU mM<sup>-1</sup>) was higher than the reported value of clinical iobitridol (*i.e.* 5.0 HU mM<sup>-1</sup>),<sup>[29]</sup> one of the most widely used CT contrast agents. This fact could be due to Yb has a higher X-ray attenuation than iodine (*e.g.* X-ray absorption coefficients at 100 KeV of Yb and iodine are 3.88 cm<sup>2</sup> g<sup>-1</sup> and 1.94 cm<sup>2</sup> g<sup>-1</sup>, respectively),<sup>[30]</sup> endowing such CQDs with higher contrast performance. These results demonstrate that co-doped CQDs herein synthesized can be also used as effective contrast agents for CT imaging.

Finally, co-doped CQDs were further examined for *in vivo* MRI and CT imaging after intravenous injection of an aqueous dispersion of the co-doped CQDs into the mouse tail vein in order to track distribution and fate of these nanoprobe and to prove *in vivo* the MR and CT contrast capabilities characterized *in vitro* previously.

As can be observed in **Figure 6** (*in vivo* CT imaging) and **Figure 7** (*in vivo* MRI), after the intravenous injection of the NPs, a contrast enhancement at an early time after injection (~ 30 min) was observed in the urinary organs: bladder (Figures 6b, 6d, 6f and 7d) and kidneys (Figures 6h and 7b). It is particularly noteworthy the excellent MR contrast after injection of the co-doped CQDs not only in the bladder (Figure 7d and Supporting Information Figure S5) but also in the renal pelvis of kidneys (Figure 7b). Additionally, both CT and MR contrasts

observed after injection were clearly apparent in the kidneys, which are better-defined than before injection, and even in the ureters (see Figure 6h and Supporting Information Figure S5a), which were contrast-enhanced and visible after the injection of the co-doped CQDs. Interestingly, as shown in Figures S6b and S6d (Supporting Information) and compared to the image acquired before injection (Supporting Information Figures S6a and S6c), a higher MR image contrast was also found in kidneys, specifically at the renal pelvis region (see Supporting Information Figure S6d), after an intraperitoneal injection of the NPs in the mouse. Furthermore, cross-validation between MRI and CT imaging results further confirmed that the co-doped CQDs entered the blood circulation of mice immediately after injection, being accumulated into the urinary organs what suggests rapid elimination of such nanoparticulated contrast agents. On the other hand, the possibility of tracking the co-doped CQDs by MRI and CT imaging while maintaining their efficient contrast capabilities after the internalization of NPs into mice seems to indicate their considerable long-term *in vivo* stability. Thus, all these *in vitro* and *in vivo* studies presented herein point out the outstanding capabilities of the CQDs co-doped with N, Gd and Yb to act not only as positive-contrast agents in MRI and CT imaging techniques separately, but also as novel nanoprobes for *in vivo* multimodal imaging.

### 3. Conclusion

In brief, synthesis of Carbon Quantum Dots by a simple one-pot microwave-assisted hydrothermal method in the presence of Gd and Yb, using citric acid and ethylenediamine as carbon and nitrogen source respectively, resulted in co-doped nanomaterials exhibiting strong fluorescence and high MR and CT contrast capabilities.

The developed nanoparticles were successfully evaluated as multimodal imaging nanoparticles being useful as imaging contrast agents for *in vitro* fluorescence cell imaging and both *in vitro* and *in vivo* MRI and CT imaging. The excellent physiological stability of

the synthesized nanoparticles, without showing appreciable cytotoxicity even at relatively high concentrations, along with the intense fluorescence (showing excellent quantum yields of 66±7%) and the outstanding contrast efficiency in MRI and CT imaging, demonstrated both in vitro and in vivo, make such CQDs co-doped with N, Gd and Yb potential contrast agents for multimodal imaging.

Based on their inherent magnetic and optical properties, the accumulation of the co-doped CQDs in the urinary organs after intravenous injection was imaged by in vivo MR and CT bimodal imaging, both of which revealed a high loading of the NPs in kidneys, ureters and, even, in the bladder.

This work constitutes a simple approach to obtain carbon-based nanoparticles, with high stability in biological media, exhibiting valuable contrast properties for multimodal bioimaging and encourages further exploration for their application in nanobiomedicine. Actually, the demonstrated advantageous multimodal contrast features of the here-synthesized doped CQDs could be also further exploited for imaging-guided targeting. For such purpose, it is required the use of appropriate targeting moieties that should be anchored on the surface of the doped CQDs forming specific interactions with a particular biomarker, thus allowing long-term post-injection imaging-guided targeting as long as ensuring their gradual release via excretion, minimizing their accumulation in organs, tumors, etc. In this context, the use of analytical platforms based on the coupling of adequate separation systems such as AF4 with elemental detectors (ICP-MS/MS) has been recently proposed<sup>[31]</sup> for the control of the functionalization of nanoparticles containing a metallic element (i.e. lanthanides doped carbon dots) with specific antibodies. Such an approach would be perfectly suited to assess and optimize the future functionalization of the here proposed doped carbon quantum dots.

#### 4. Experimental Section

*Material Synthesis:* Carbon Quantum Dots (CQDs) co-doped with N, Gd and Yb were synthesized *via* one-pot microwave-assisted hydrothermal treatment of citric acid and ethylenediamine, used as carbon precursor and passivation agent respectively, in presence of both lanthanide precursors as doping ions ( $\text{Gd}^{3+}$  and  $\text{Yb}^{3+}$ ). Briefly, 0.45 g of citric acid, 0.15 g of a  $\text{Gd}^{3+}$  complex, 0.1 g  $\text{YbCl}_3$  and 0.5 mL ethylenediamine were added into a beaker and sequentially dispersed into 10 mL Milli-Q water under stirring. After 10 min of ultrasonic mixing to get a homogeneous solution, this aqueous solution was placed into a Teflon-lined ETHOS 1 Microwave Labstation system (Milestone, Italy) and heated to 180 °C for 4 h (at 850 W). After cooling to room temperature, a dark solution containing the co-doped CQDs was obtained. The obtained solution was purified by dialysis against Milli-Q water using a 2 kDa cut-off dialysis cassette for 24 h (Milli-Q water was changed during dialysis every 3 h). The resultant aqueous solution containing the co-doped CQDs was filtered through a 0.22 µm PVDF membrane filter to remove possible residual particles. After purification process, a light brown aqueous solution containing the co-doped CQDs was obtained for their later characterization and application.

*NPs characterization:* Transmission electron microscopy was performed in a JEOL JEM 2100 (JEOL, Japan) equipped with an Oxford INCA X-ray microanalysis system. For the HR-TEM investigations, 5 µL of the co-doped CQDs was drop casted onto a 300 mesh carbon coated copper grid (Agar Scientific, United Kingdom) and air dried. XRD measurements were performed using an X'Pert Pro MPD diffractometer (PANalytical, Netherlands). For microstructural analysis of the synthesized co-doped CQDs, X-ray powder diffraction measurements were performed employing the X'Pert Pro diffractometer with Bragg–Brentano configuration, a monochromatic  $\text{Cu K}_{\alpha}$  radiation ( $\lambda = 1.5418 \text{ \AA}$ ) and a PIXcel detector. The powder sample was placed on a zero background silicon holder and the XRD pattern from 5°

to 85° (2θ) was recorded at room temperature with a step size of 0.0131° and a counting time of 180 s per step. Infrared spectrum was taken in a Varian 670 FT-IR spectrometer (Agilent, Australia) equipped with a Golden Gate attenuated total reflectance (ATR) device consisted of a diamond crystal with one internal reflection.

UV-vis spectrophotometric measurements were performed in a Genesys 10S Spectrophotometer (Thermo Scientific, Germany). Fluorescence emission and quantum yield (QY) of the CQDs co-doped with N, Gd and Yb was measured using a Varian Cary Eclipse fluorescence spectrophotometer (Agilent, USA) and a LS-50B Luminescence Spectrometer (Perkin Elmer, USA), ensuring a fixed excitation wavelength of 350 nm, with both excitation and emission slits width of 5 nm. Fluorescence measurements were carried out using conventional Quartz SUPRASIL cuvettes (Hellma Analytics, Germany). QY of the co-doped CQDs was calculated by the following equation (**Equation 1**):

$$QY = QY_R \frac{I}{I_R} \frac{A_R}{A} \frac{n^2}{n_R^2} \quad (1)$$

where  $QY_R$  is the fluorescence quantum yield of the reference;  $I$  and  $I_R$  are the measured integrated fluorescence emission intensities of the co-doped CQDs and the reference, respectively;  $A$  and  $A_R$  are the absorbance values at the excitation wavelength (350 nm) of the co-doped CQDs and the reference, respectively; and  $n$  is the refractive index ( $n_{\text{water}} = 1.33$ ). Quinine sulfate in 0.5 M H<sub>2</sub>SO<sub>4</sub> was used as reference ( $QY_{\text{quinine}} = 54.6\%$ ). In order to avoid internal filter effects and minimize reabsorption, the absorbance values of the co-doped CQDs and the reference at the excitation wavelength were kept below 0.10. In addition, a FS5 Spectrofluorometer (Edinburgh Instruments, UK) provided the fluorescence lifetime of the co-doped CQDs (a 405 nm laser excitation was used and the fluorescence emission was monitored at 440 nm).

The different metal concentrations in the CQDs co-doped with N, Gd and Yb were determined by ICP-MS. Elemental measurements were carried out on a 8800 triple quadrupole ICP-MS, ICP-QQQ (Agilent Technologies, Japan), using a MicroMist nebulizer. The use of the triple quadrupole ICP-MS allowed the interference-free detection of the different elements present in the co-doped CQDs (*i.e.* Gd and Yb). Oxygen was introduced in the collision/reaction cell at a flow of 0.35 mL min<sup>-1</sup>. Thus, Gd was detected in mass-shift MS/MS mode ( $^{157}\text{Gd}^+ \rightarrow ^{173}\text{GdO}^+$ ), after their reaction with oxygen in the cell, and Yb was measured in on-mass mode ( $^{172}\text{Yb}^+ \rightarrow ^{172}\text{Yb}^+$ ), since Yb does not react with oxygen. The operation conditions were daily optimized using a tuning solution. Moreover, an ultrasonic bath (JP Selecta, Spain) was used to improve the acid digestion of the co-doped CQDs before ICP-MS analysis.

*Cell viability assay and cell imaging:* Cell viability of CQDs co-doped with N, Gd and Yb was evaluated by MTT reduction assay on three different well-established cell lines: human cervical carcinoma HeLa cells, mouse embryonic fibroblast NIH-3T3 cells and Chinese hamster ovary (CHO) cells. Cells (1500 cells per well) were seeded in 96-well plates, incubated at 37 °C in a humidified 5 % CO<sub>2</sub> environment and left to attach overnight. Then, cells were treated with different concentrations of co-doped CQDs (0, 0.2, 2, 20, 200 and 2000 µg/mL) for 24 h and 72 h. After treatment, MTT reagent was added to each well. Three hours later, cells were lysed by adding the lysis buffer and left for 6 h at 37 °C in the dark. Absorbance at 570 nm was measured using a Cary 50-MPR microplate reader (Agilent Technologies, USA). Results are shown as the average of six samples ± SD.

A Leica TCS-SP8X confocal microscope (Leica, Germany) was used to visualize the distribution and the cellular uptake of the co-doped CQDs in the different cells lines used (*i.e.* HeLa, NIH-3T3 and CHO cells). For confocal microscopy study, cells (60000 cells per well) were seeded and grown on sterile Nunc™ Thermanox™ coverslips previously placed in 6-

well plates. Then, cells were incubated with the co-doped CQDs at a concentration of 200 µg/mL for 24 h. After treatment, cells were washed thoroughly with PBS and, immediately, fixed with 4% formaldehyde in PBS. Cells were then rinsed with PBS and, finally, the coverslips were mounted using Fluoromount-G. The confocal fluorescent microscopic images of the cells were taken under a 405 nm diode laser excitation and *ImageJ* program (Bethesda, MD, USA) was used for image processing.

*In vitro and in vivo MRI measurements:* *In vitro* MRI experiments were performed on a 7-T Bruker Biospec 70/30 USR MRI system (Bruker, Germany), interfaced to an AVANCE III console. The BGA12 imaging gradient (maximum gradient strength 400 mT/m) and a 40mm diameter quadrature volume resonator were used. For T<sub>1</sub> maps imaging of the phantoms the following parameters were adopted: Spin echo saturation recovery using a variable repetition time Bruker's RAREVTR method. Images were acquired at 20 different TR values (from 46 to 8000 ms), TE 8 ms, RARE factor 1. For T<sub>2</sub> maps imaging of the phantoms the following parameters were adopted: Bruker's MSME (Multi slice Spin echo) sequence was used. The TE values were varied in 64 steps ranging from 12 ms to 768 ms and TR 15 s. All data were acquired with 2 averages, 256 x 256 points and a Field of View of 2.56 cm x 2.56 cm, 3 slices with a slice thickness of 2.0 mm and 5 mm gap between slices. The images were fitted into Levenberg-Margardt method to calculate T<sub>1</sub> and T<sub>2</sub> values using Bruker's Paravision 6.0.1 software.

For *in vivo* MRI imaging, a BioSpec 70/20 USR MRI system (Bruker, Germany) was used. RARE (Rapid Acquisition with Refocused Echo) sequence was used. The TR/TE values were 1500/6.5 and all data were acquired with 2 averages, a matrix size was 256 x 256 points, a Field of View of 40 mm x 80 mm, a slice thickness of 0.5 mm and 0.75 mm space between slices. Before MRI analysis, mice were anesthetized using isoflurane. Then, a solution of co-doped CQDs at a Gd concentration of 7 mM were administered into two mice *via* an

intravenous injection into the mouse tail vein (200  $\mu\text{L}$ ) and an intraperitoneal injection (350  $\mu\text{L}$ ), respectively. After the contrast administration, mice were imaged by the MRI system.

*In vitro and in vivo CT measurements:* For *in vitro* CT measurements, all samples were scanned by high resolution micro-computed tomography using a SkyScan 1174 (Bruker, Belgium). The small sample holder device for  $\mu\text{CT}$  was used to fit the specimen with the long axis perpendicular to the floor of the specimen holder and the X-ray source. Images were obtained by 50 kV X-ray tube voltage and 800  $\mu\text{A}$ . All specimens were scanned at 29.8  $\mu\text{m}$  pixel size resolution. For each specimen, a series of 315 projection images were obtained with a rotation step of 0.6° and frame averaging 2 for a total 180° rotation. The scanning time for each sample was approximately 16 minutes using an exposure time of 1250 ms. Flat field correction was performed at the beginning of each scan. The images obtained during scanning were reconstructed using the software NRecon (SkyScan). The correction values of attenuation coefficient, beam hardering, smoothing and ring-artifact reduction were the same in all samples. For performance calibration on Hounsfield units (HU), it was used the software provided by the manufacturer (CTAn). Volume of interest (VOI) was manually delimited in each of the samples (300 slices were chosen).

For *in vivo* CT imaging, an Argus PET-CT scanner (SEDECAL, Spain) was used. *In vivo* CT images were obtained in high resolution using 45 kV and 300  $\mu\text{A}$ . Before CT analysis, the mouse was anesthetized using isoflurane. Then, 200  $\mu\text{L}$  of co-doped CQDs at a Yb concentration of 10 mM was intravenously injected into the mouse tail vein and imaged by the CT system.

## Supporting Information

Supporting Information is available from the Wiley Online Library or from the author.

## Acknowledgements

This research work was supported by the Spanish Ministry of Education through the project MINECO-17-CTQ2016-79412-P and by Principado de Asturias (Spain) through the project GRUPIN IDI/2018/000166. Diego Bouzas-Ramos acknowledges the Ph.D. grant (BP14-137) from Principado de Asturias (Spain).

Received: ((will be filled in by the editorial staff))

Revised: ((will be filled in by the editorial staff))

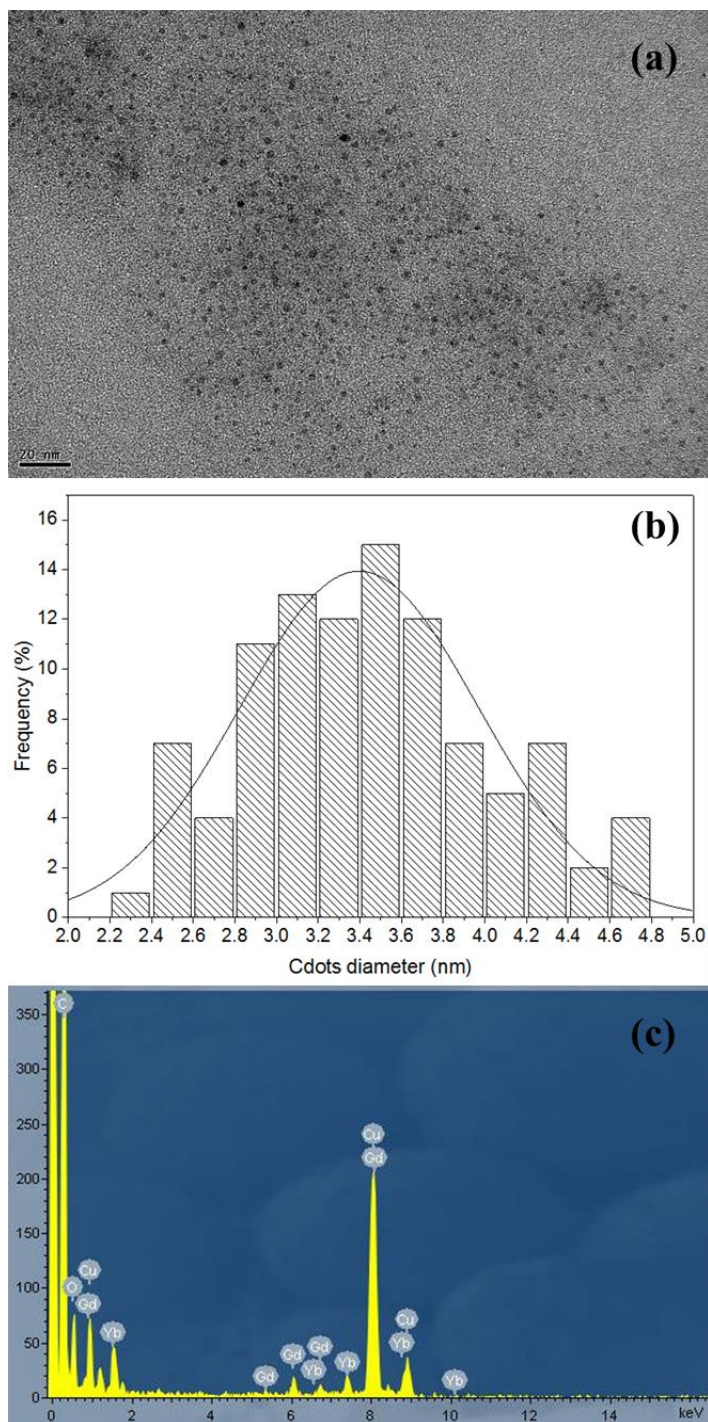
Published online: ((will be filled in by the editorial staff))

## References

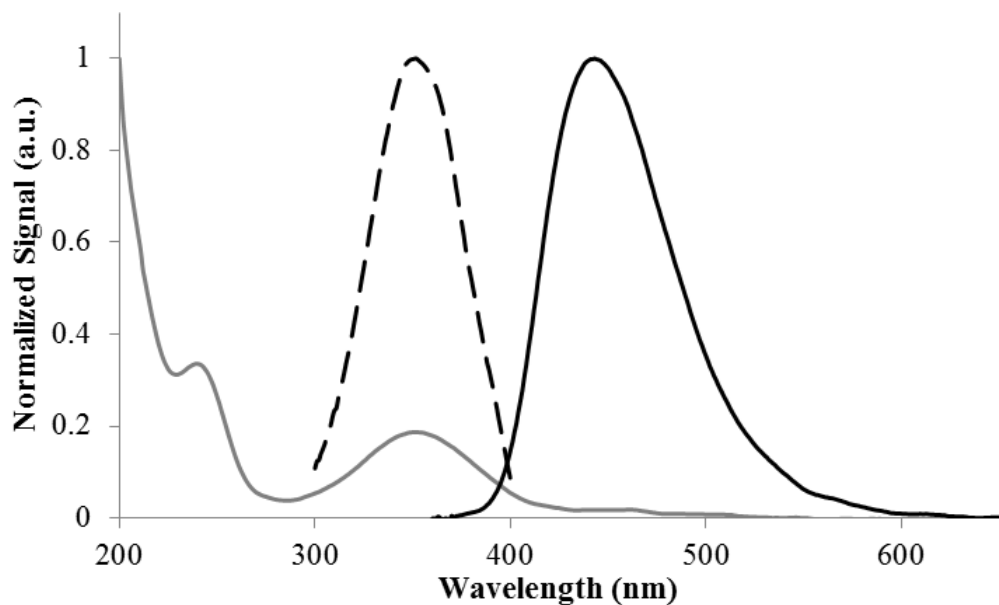
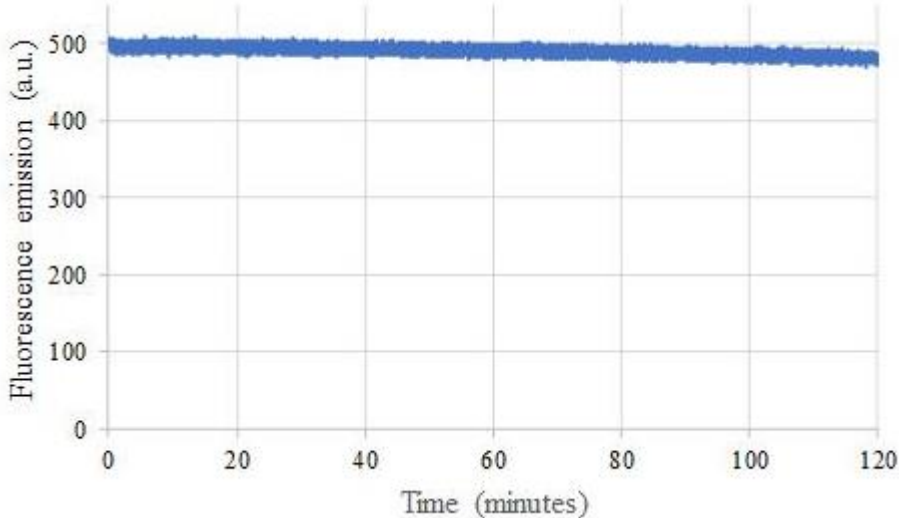
- [1] D.-E-. Lee, H. Koo, I.-C. Sun, J. H. Ryu, K. Kim, I. C. Kwon, *Chem. Soc. Rev.* **2012**, *41*, 2656.
- [2] J. Key, J. F. Leary, *Int. J. Nanomed.* **2014**, *9*, 711.
- [3] J. Rieffel, U. Chitgupi, J.F. Lovell, *Small* **2015**, *11*, 4445.
- [4] J. Kim, P. Chour, J. Hsu, H. I. Litt, V. A. Ferrari, R. Popovtzer, D. P. Cormode, *Bioconjugate Chem.* **2017**, *28*, 1581.
- [5] O. S. Wolfbeis, *Chem. Soc. Rev.* **2015**, *44*, 4743.
- [6] G. Chen, T. Y. Ohulchanskyy, W. C. Law, H. Agren, P. N. Prasad, *Nanoscale* **2011**, *3*, 2003.
- [7] A. Xia, M. Chen, Y. Gao, D. Wu, D. Feng, F. Li, *Biomaterials* **2012**, *33*, 5394.
- [8] R. Lv, P. Yang, F. He, S. Gai, C. Li, Y. Dai, G. Yang, J. Lin, *ACS Nano* **2015**, *9*, 1630.
- [9] L. Feng, F. He, Y. Dai, C. Zhong, C. Li, P. Yang, *Biomater. Sci.* **2017**, *5*, 2456.

- [10] K. Hola, Y. Zhang, Y. Wang, E.P. Giannelis, R. Zboril, A.L. Rogach, *Nano Today* **2014**, *9*, 590.
- [11] S. Zhu, X. Zhao, Y. Song, S. Lu, B. Yang, *Nano Today* **2016**, *11*, 128.
- [12] A. Cayuela, M.L. Soriano, C. Carrillo-Carrión, M. Valcárcel, *Chem. Commun.* **2016**, *52*, 1311.
- [13] P.G. Luo, S. Sahu, S. Yang, S.K. Sonkar, J. Wang, H. Wang, G.E. LeCroy, L. Cao, Y. Sun, *J. Mater. Chem. B* **2013**, *1*, 2116.
- [14] S. Zhu, Q. Meng, L. Wang, J. Zhang, Y. Song, H. Jin, K. Zhang, H. Sun, H. Wang, B. Yang, *Angew. Chem. Int. Ed.* **2013**, *52*, 3953.
- [15] H. Chen, L. Wang, H. Fu, Z. Wang, Y. Xie, Z. Zhang, Y. Tang, *J. Mater. Chem. B* **2016**, *4*, 7472.
- [16] F. Du, L. Zhang, L. Zhang, M. Zhang, A. Gong, Y. Tan, J. Miao, Y. Gong, M. Sun, H. Ju, C. Wu, S. Zou, *Biomaterials* **2017**, *121*, 109.
- [17] J. Gallo, N. Vasimalai, M.T. Fernandez-Arguelles, M. Bañobre-López, *Dalton Trans.* **2016**, *45*, 17672.
- [18] L. Tang, R. Ji, X. Cao, J. Lin, H. Jiang, X. Li, K. Seng Teng, C. Man Luk, S. Zeng, J. Hao, S. Ping Lau, *ACS Nano* **2012**, *6*, 5102.
- [19] H. Gonçalves, J. C. G. Esteves da Silva, *Acid, J Fluoresc* **2010**, *20*, 1023.
- [20] J.I. Murray, M.L. Whitfield, N.D. Trinklein, R.M. Myers, P.O. Brown, D. Botstein, *Mol. Biol. Cell* **2004**, *15*, 2361.
- [21] K. Wissel, G. Brandes, N. Pütz, G.L. Angrisani, J. Thieleke, T. Lenarz, M. Durisin, *PLOS One* **2018**, *13*[5]: e0196649.

- [22] S. Pereira, H.F. Kildegaard, M.R. Andersen, *Biotechnol. J.* **2018**, *13*, 1700499.
- [23] L.W. Zhang, N.A. Monteiro-Riviere, *Toxicol. Sci.* **2009**, *110*, 138.
- [24] P. Caravan, J.J. Ellison, T.J. McMurry R.B. Lauffer, *Chem. Rev.* **1999**, *99*, 2293.
- [25] Y. Shen, F.L. Goerner, C. Snyder, J.N. Morelli, D. Hao, D. Hu, X. Li, V.M. Runge, *Invest. Radiol.* **2015**, *50*, 330.
- [26] T. Sh. Atabaev, *Nanomaterials* **2018**, *8*, 342.
- [27] J.R. Morrow, E. Toth, *Inorg. Chem.* **2017**, *56*, 6029.
- [28] Z. Liu, Z. Li, J. Liu, S. Gu, Q. Yuan, J. Ren, X. Qu., *Biomaterials* **2012**, *33*, 6748.
- [29] J. Sui, G. Liu, Y. Song, D. Li, X. Dong, J. Wang, W. Yu, *J. Colloid Interface Sci.* **2018**, *510*, 292.
- [30] D. Ni, W. Bu, S. Zhang, X. Zheng, M. Li, H. Xing, Q. Xiao, Y. Liu, Y. Hua, L. Zhou, W. Peng, K. Zhao, J. Shi, *Adv. Funct. Mater.* **2014**, *24*, 6613.
- [31] D. Bouzas-Ramos, J. I. García-Alonso, J. M. Costa-Fernández, J. Ruiz Encinar, *Anal. Chem.* **2019**, *91*, 3567.



**Figure 1.** (a) HR-TEM image, (b) size distribution histogram and (c) EDX analysis of CQDs co-doped with N, Gd and Yb.

**a)****b)**

**Figure 2. a)** UV-vis absorption (solid gray line), fluorescence emission by excitation at 350 nm (solid black line) and related excitation spectra (dashed black line) of the CQDs co-doped with N, Gd and Yb. **b)** Fluorescence emission intensity registered at 450 nm (arbitrary units) from the CQDs continuously excited at 350 nm.

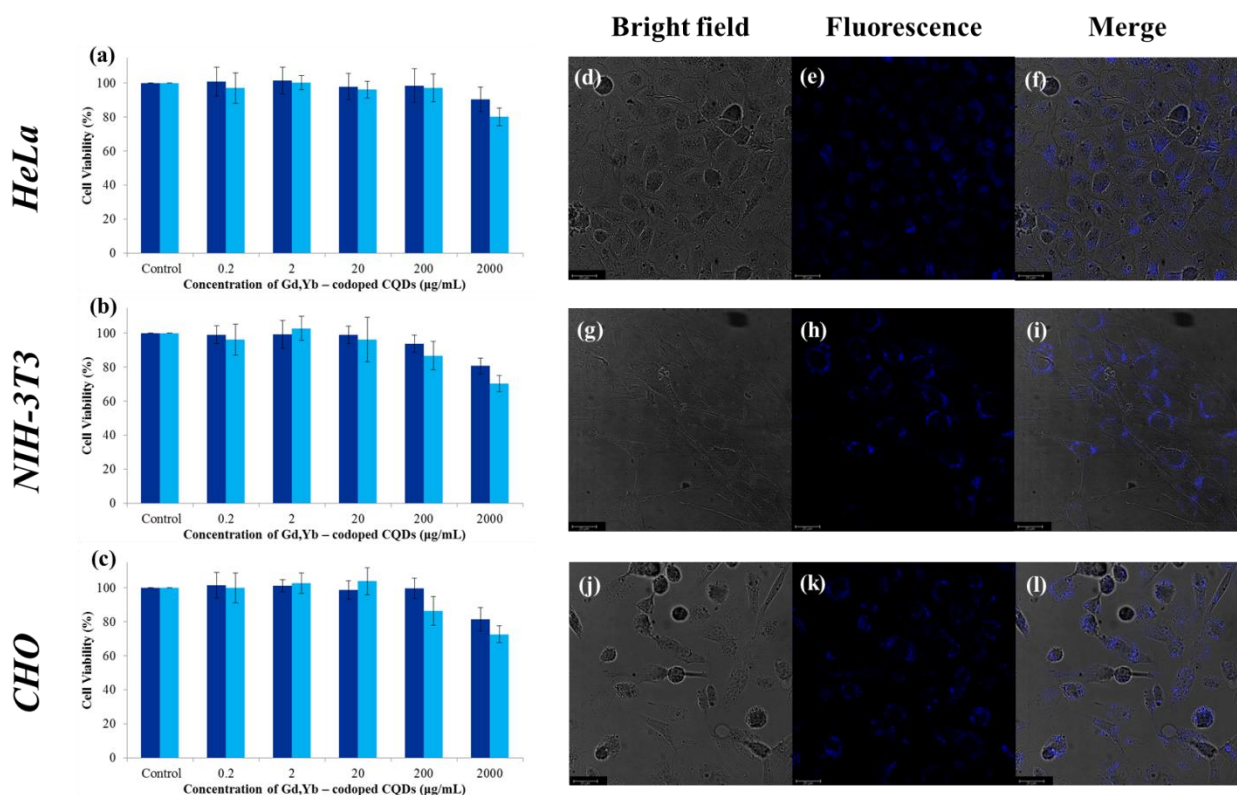


**Figure 3.** Cell viability values of (a) HeLa, (b) NIH-3T3 and (c) CHO cells incubated at 37 °C for 24 h (dark blue bars) and 72 h (light blue bars) with different concentrations of co-doped CQDs (0, 0.2, 2, 20, 200 and 2000 μg/mL). Confocal fluorescence images of (d, e, f) HeLa, (g, h, i) NIH-3T3 and (j, k, l) CHO cells treated with such CQDs at a concentration of 200 μg/mL for 24 h. Images were taken under (d, g, j) bright field, (e, h, k) fluorescence at an excitation wavelength of 405 nm, and (f, i, l) merge of corresponding bright field and fluorescence images (scale bar = 20 μm).

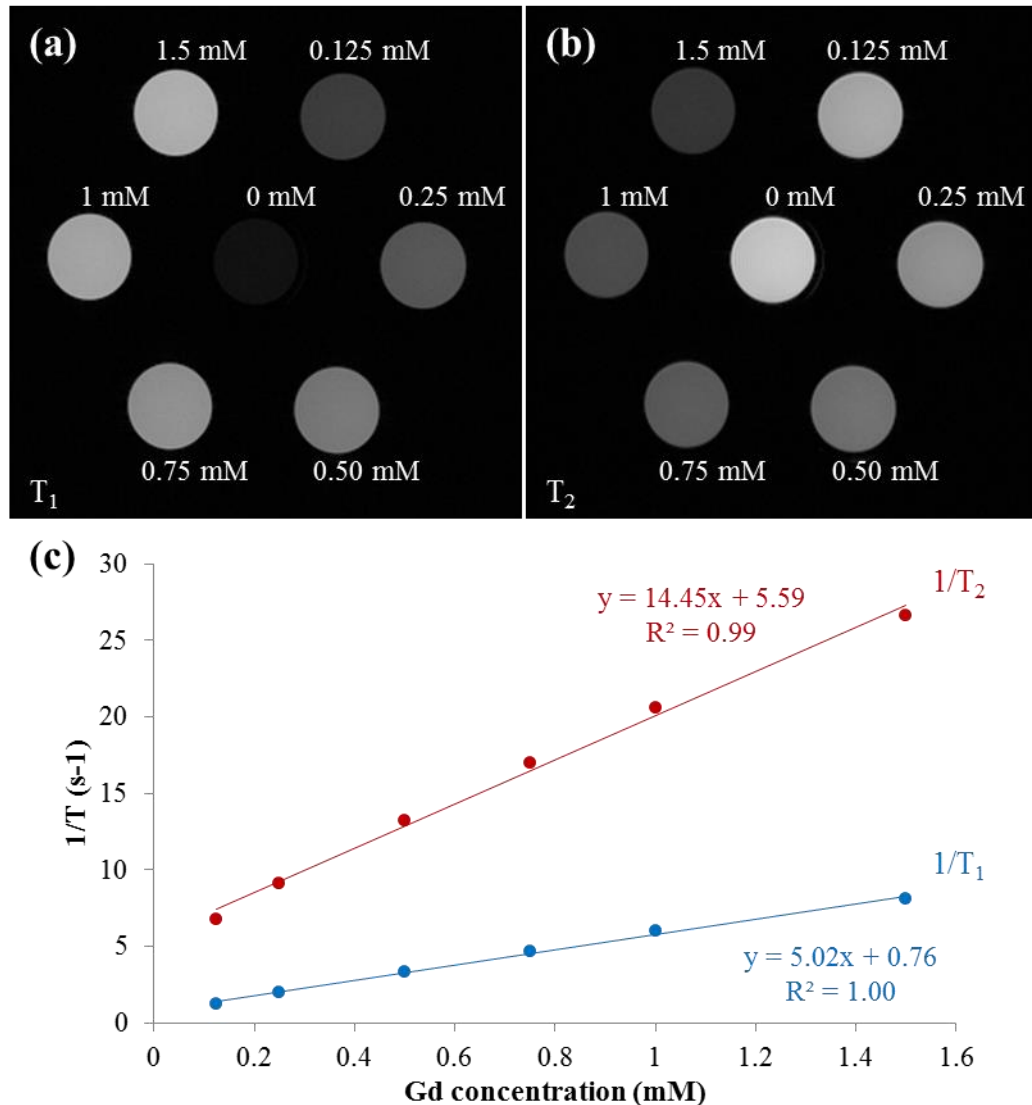


**Figure 4.** (a) T<sub>1</sub>-weighted and (b) T<sub>2</sub>-weighted MR phantom images of CQDs co-doped with N, Gd and Yb at various concentrations of Gd. (c) Linear relationships of longitudinal,  $1/T_1$  (curve in blue), and transverse,  $1/T_2$  (curve in red), relaxation rates of such CQDs as a function of different concentrations of Gd. Precision associated to every individual point below 1 % RSD.

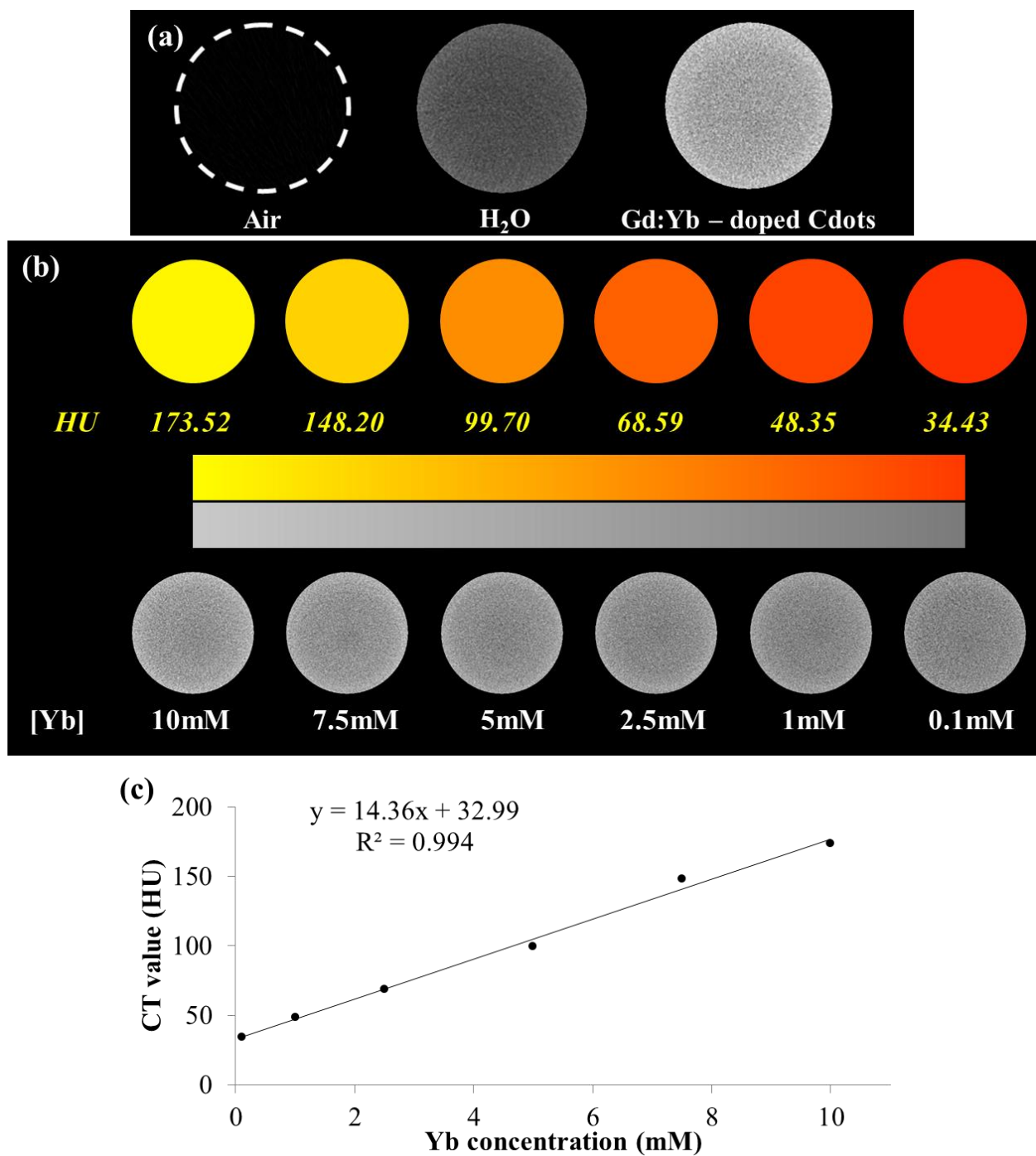


**Figure 5.** (a) CT phantom images of air, water and an aqueous solution of CQDs co-doped with N, Gd and Yb. (b) *In vitro* CT images and color-mapped images as function of different concentrations of Yb. (c) CT value (HU) versus different concentrations of Yb. Precision associated to every individual point below 1 % RSD.

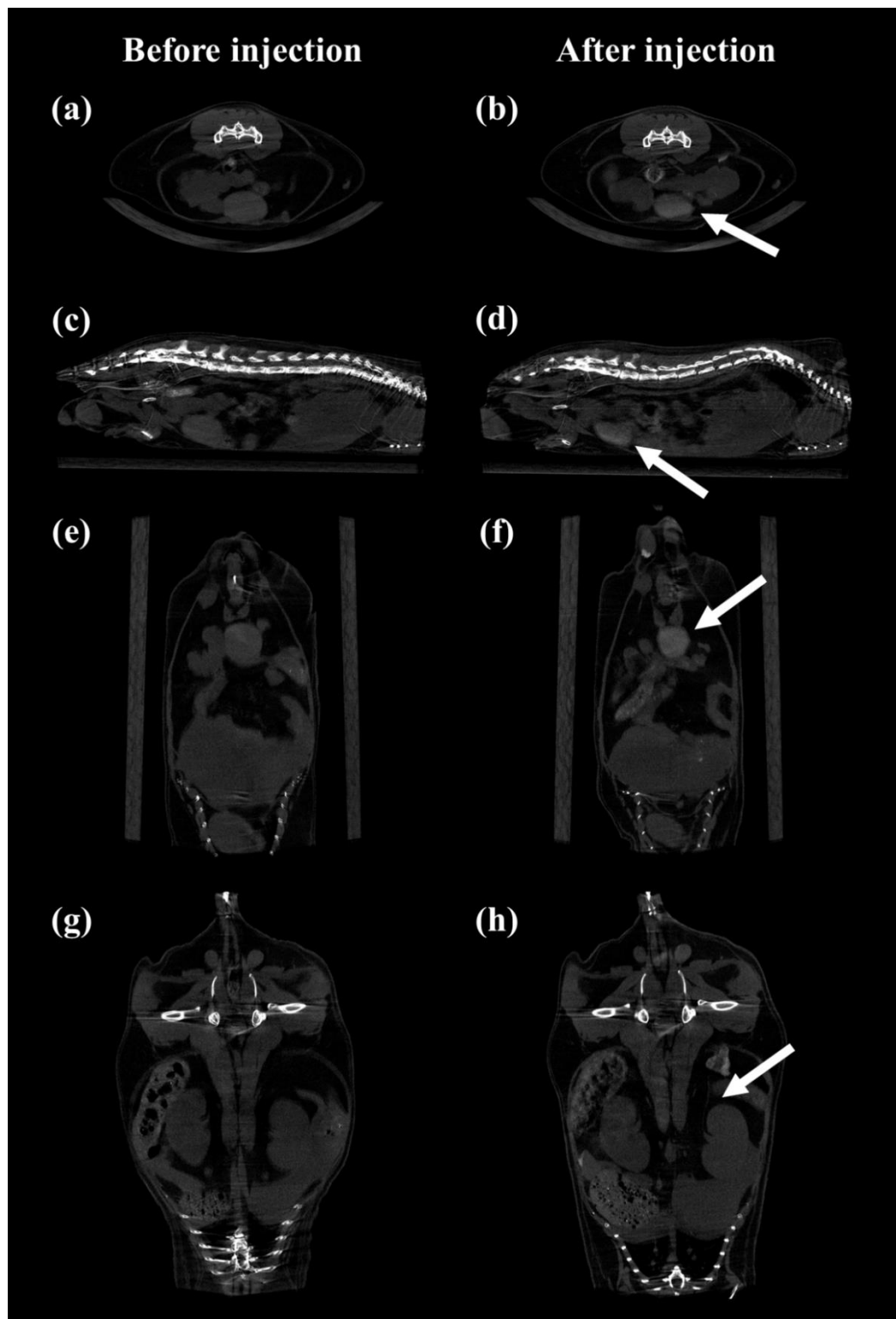


**Figure 6.** *In vivo* CT (a, b) axial, (c, d) sagittal and (e-h) coronal images of a mouse (a, c, e, g) before injection and (b, d, f, h) after intravenous tail vein injection of CQDs co-doped with N, Gd and Yb. Arrows point the contrast-enhanced regions observed at an early time after injection ( $\sim 30$  min).

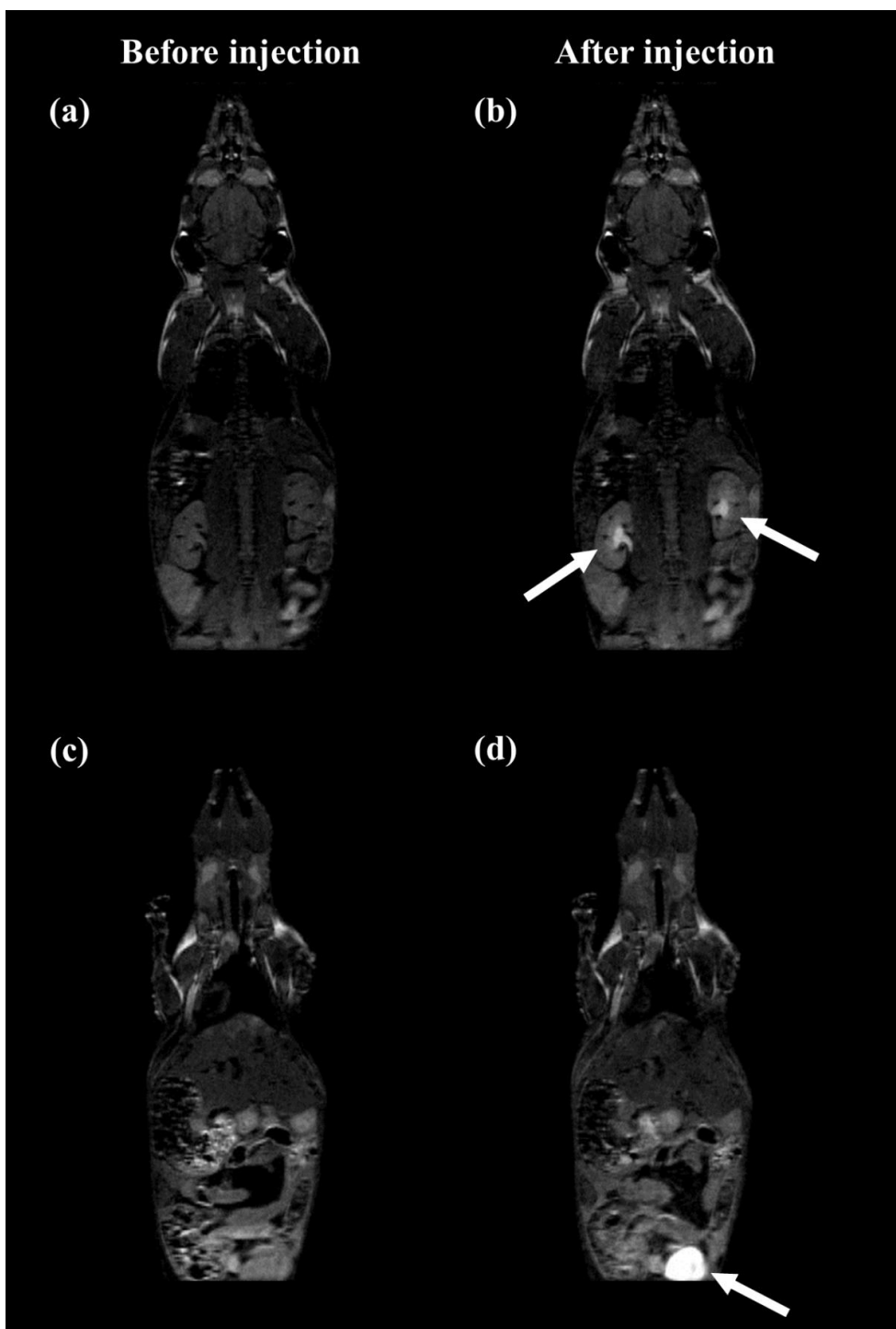


**Figure 7.** *In vivo* MRI coronal images of a mouse (a, c) before injection and (b, d) after intravenous tail vein injection of CQDs co-doped with N, Gd and Yb. Arrows point the contrast-enhanced regions observed at an early time after injection (~ 30 min).

**Table of contents entry**

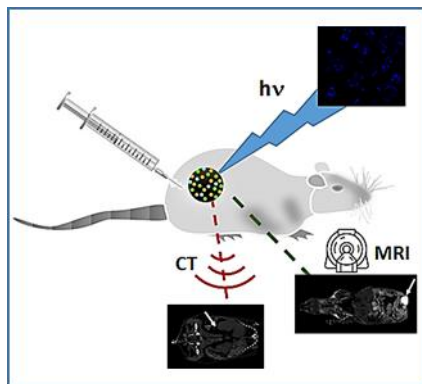
**Carbon Quantum Dots co-doped with nitrogen and lanthanides are synthesized and evaluated for multimodal imaging.** Such doped nanomaterials constitute an ideal platform for multimodal imaging as they exhibit strong fluorescence, magnetic resonance and computed tomography contrast properties. Potential applicability of the multimodal nanoparticles are demonstrated for both *in vitro* and *in vivo* bioimaging.

**Keywords** doped nanoparticles, carbon quantum dots, multimodal imaging, *in vitro* imaging, *in vivo* imaging

**Authors** D. Bouzas-Ramos, J. Cigales Canga, J. C. Mayo\*, R. M. Sainz, J. Ruiz Encinar, J. M. Costa-Fernandez\*.

**Title** Carbon Quantum Dots co-Doped with Nitrogen and Lanthanides for Multimodal Imaging

**ToC figure** ((Please choose one size: 55 mm broad × 50 mm high **or** 110 mm broad × 20 mm high. Please do not use any other dimensions))



Copyright WILEY-VCH Verlag GmbH & Co. KGaA, 69469 Weinheim, Germany, 2016.

## Supporting Information

**Title:** Carbon Quantum Dots co-Doped with Nitrogen and Lanthanides for Multimodal Imaging

*Author(s), and Corresponding Author(s)\** Diego Bouzas-Ramos, Jesus Cigales Canga, Juan Carlos Mayo\*, Rosa Maria Sainz, Jorge Ruiz Encinar, Jose M. Costa-Fernandez\*.

### I. Chemicals, Materials and Cell Culture.

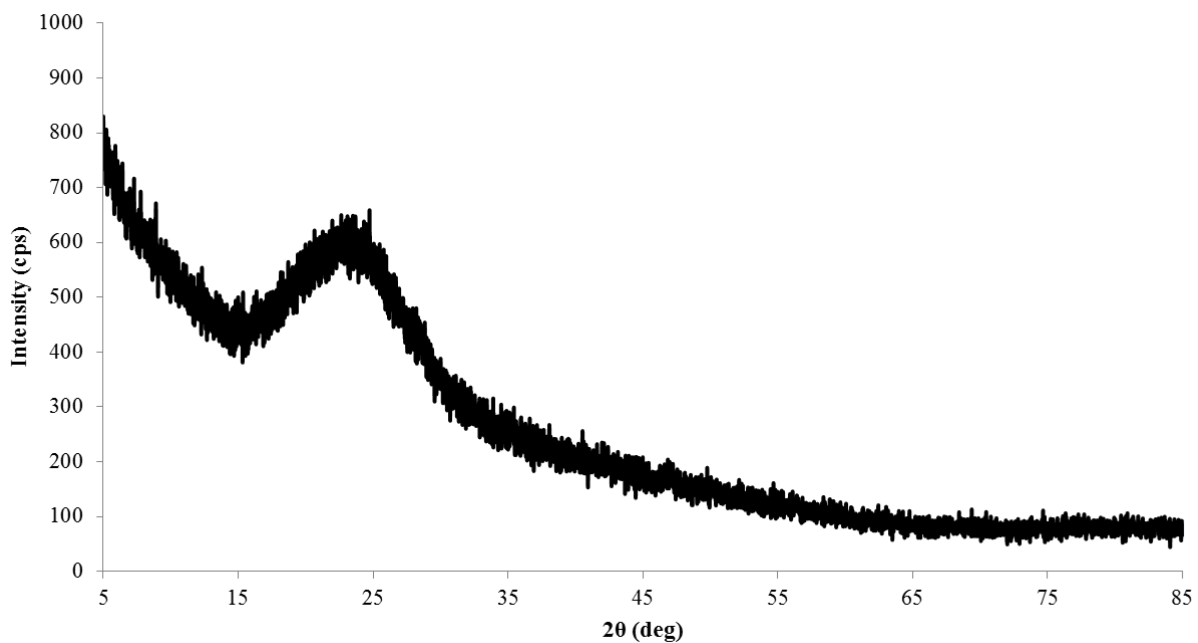
All the chemical reagents used in the experiments were of analytical grade and used as received without further purification. Deionized ultrapure water ( $18.2 \text{ M}\Omega \text{ cm}$ ) was obtained with a Milli-Q system (Millipore; Bedford, MA, USA) and it was used throughout the present work.

The precursors used for the synthesis of the Carbon Quantum Dots (CQDs) co-doped with N, Gd and Yb were citric acid monohydrate ( $\geq 99\%$ ), ethylenediamine ( $\geq 99\%$ ), diethylenetriaminepentaacetic acid gadolinium(III) dihydrogen salt hydrate (97 %) and ytterbium(III) chloride hexahydrate (99.9 %), all of them purchased from Sigma-Aldrich (Milwaukee, WI, USA). For dialysis purification of the co-doped CQDs, 15 mL dialysis cassettes (2 kDa cut-off) were used and purchased from Thermo Scientific (Rockford, IL, USA). Merck (Darmstadt, Germany) certified 1000 mg/L standards of Gd and Yb were used in the ICP-MS analysis.

Human cervical carcinoma HeLa cells (Cat Number # CCL-2<sup>TM</sup>) were purchased from ‘American Type Culture Collection’ (ATCC; Manassas, VA, USA), while Chinese hamster ovary (CHO) cells (Cat Number # 85050302) and mouse embryonic fibroblast NIH-3T3 cells (Cat Number # 93061524) were obtained from ‘European Collection of Cell Cultures’ (ECACC; Salisbury, UK). Cells were cultured in Dulbecco's Modified Eagle Medium (DMEM) supplemented with 10% fetal bovine serum (FBS), 2 mM L-glutamine, 10 mM HEPES and an antibiotic-antimycotic cocktail containing 100 U/mL penicillin, 10 µg/mL streptomycin and 0.25 µg/mL amphotericin B. All cell culture reagents were purchased from Gibco®-Invitrogen (Thermo Fisher Scientific; Waltham, MA, USA) unless otherwise indicated. Cell lines were grown at 37 °C in a humidified 5% CO<sub>2</sub> environment. Medium was changed every 2 days and cultures were split at least once a week before confluence.

For cell viability assays, after brief trypsinization cells were harvested, counted in a Neubauer chamber and 15000 cells/ml were seeded in 96-well plates. Before starting the experiments, cells were left attached overnight. On the other hand, for confocal microscopy study, cells were seeded at a density of 40000 cells/mL and grown on sterile Nunc<sup>TM</sup> Thermanox<sup>TM</sup> coverslips, purchased from Thermo Scientific, in a 6-well plate. Then, the coverslips were finally mounted using both Fluoromount-G, obtained from SouthernBiotech (Birmingham, AL, USA).

For *in vivo* CT studies, a thirty six-week-old male wild-type mouse was used and treated with the CQDs co-doped with N, Gd and Yb *via* an intravenous injection into the mouse tail vein. For *in vivo* MRI studies, a ten-month-old male wild-type mouse and a thirty-week-old female wild-type mouse were used and treated with co-doped CQDs *via* an intravenous injection into the mouse tail vein and an intraperitoneal injection, respectively. The inbred mouse strain of mice used during *in vivo* studies was “C57BL/6”. All procedures were approved by the ‘Institutional Animal Care and Ethical Committee’ of the University of Oviedo.

**II. SUPPLEMENTARY FIGURES.**

**Figure S1.** Powder XRD pattern of the CQDs co-doped with N, Gd and Yb.

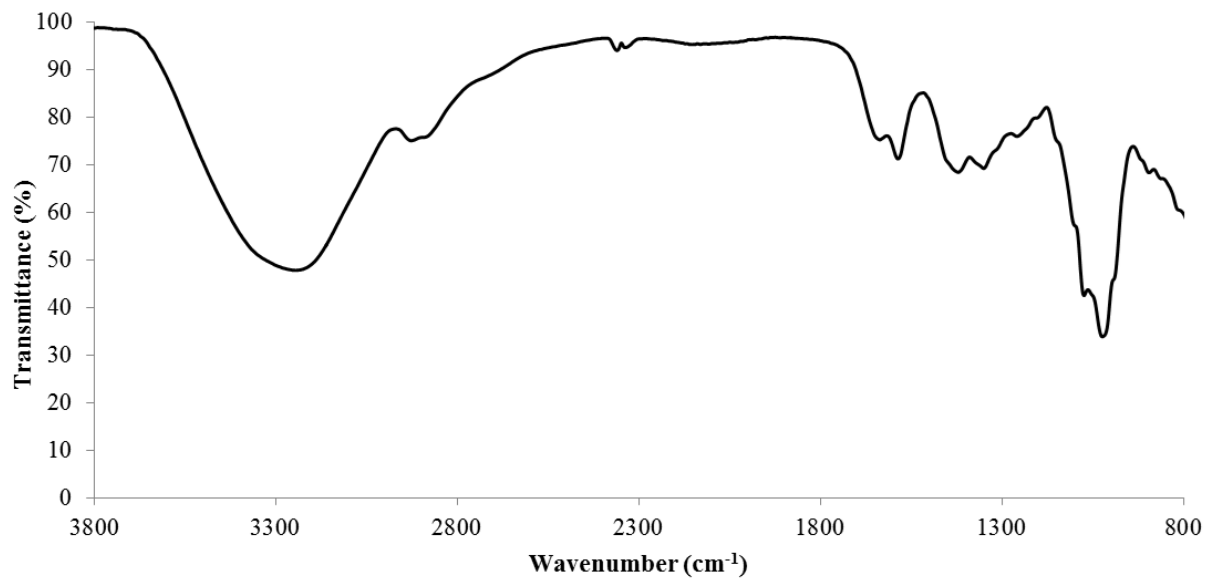


**Figure S2.** FT-IR spectrum of the CQDs co-doped with N, Gd and Yb.

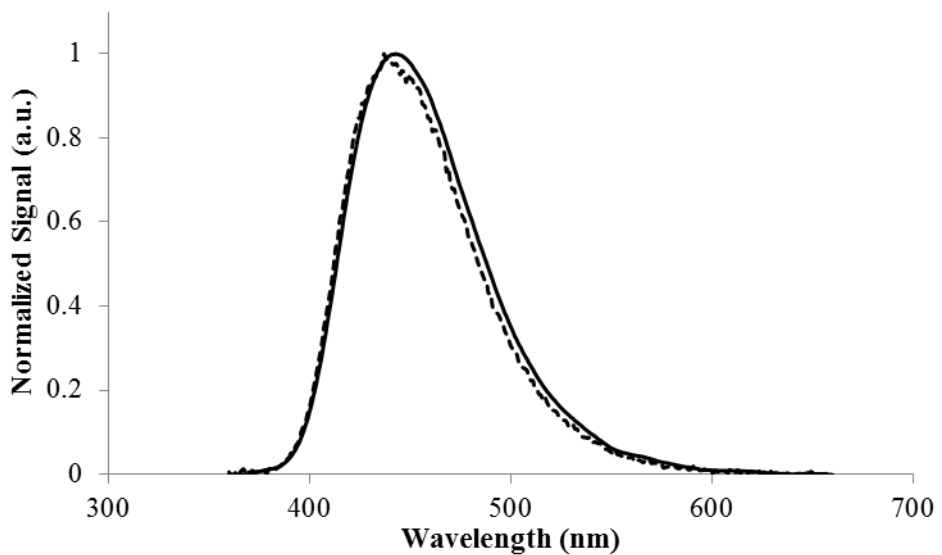


**Figure S3.** Fluorescence emission spectra by excitation at 350 nm of the CQDs co-doped with N, Gd and Yb (solid line) and the N-doped CQDs (dashed line).

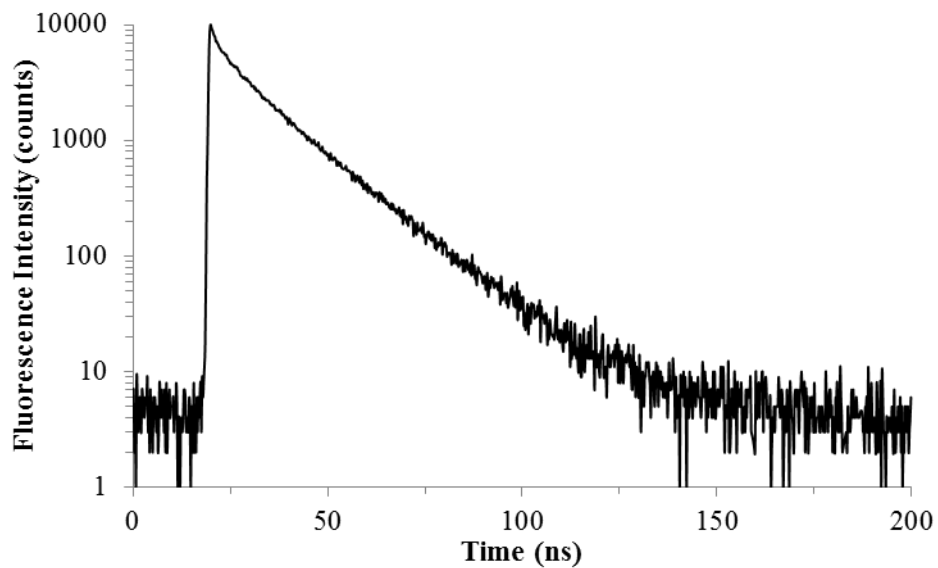


**Figure S4.** Fluorescence decay curve of the CQDs co-doped with N, Gd and Yb (405 nm laser excitation).

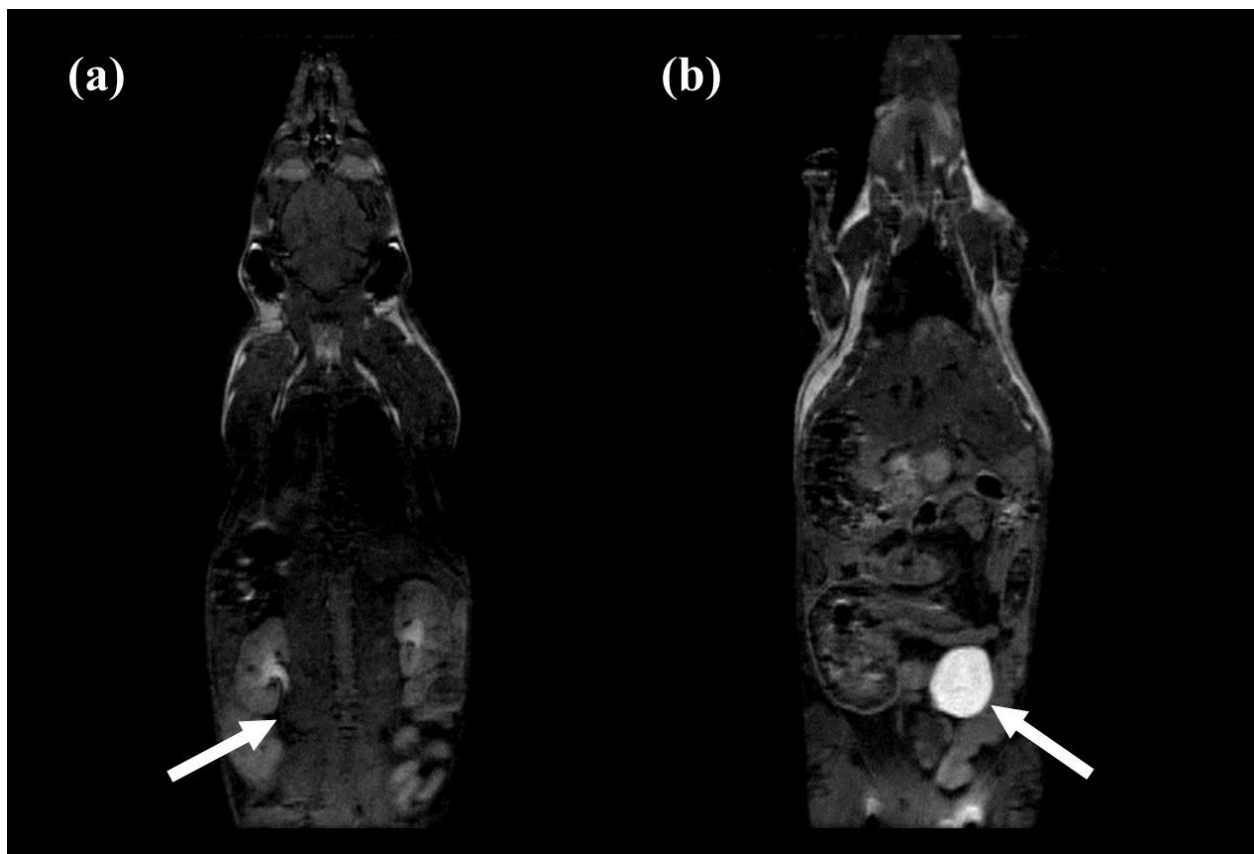


**Figure S5.** *In vivo* MRI coronal images of a mouse after intravenous tail vein injection of CQDs co-doped with N, Gd and Yb. Arrows point the contrast-enhanced regions observed at an early time after injection: (a) kidneys and ureters, and (b) bladder.

Figure S5 complements Figure 7, making more visible the contrast-enhanced observed in kidneys, ureters and bladder after injection of the co-doped CQDs.

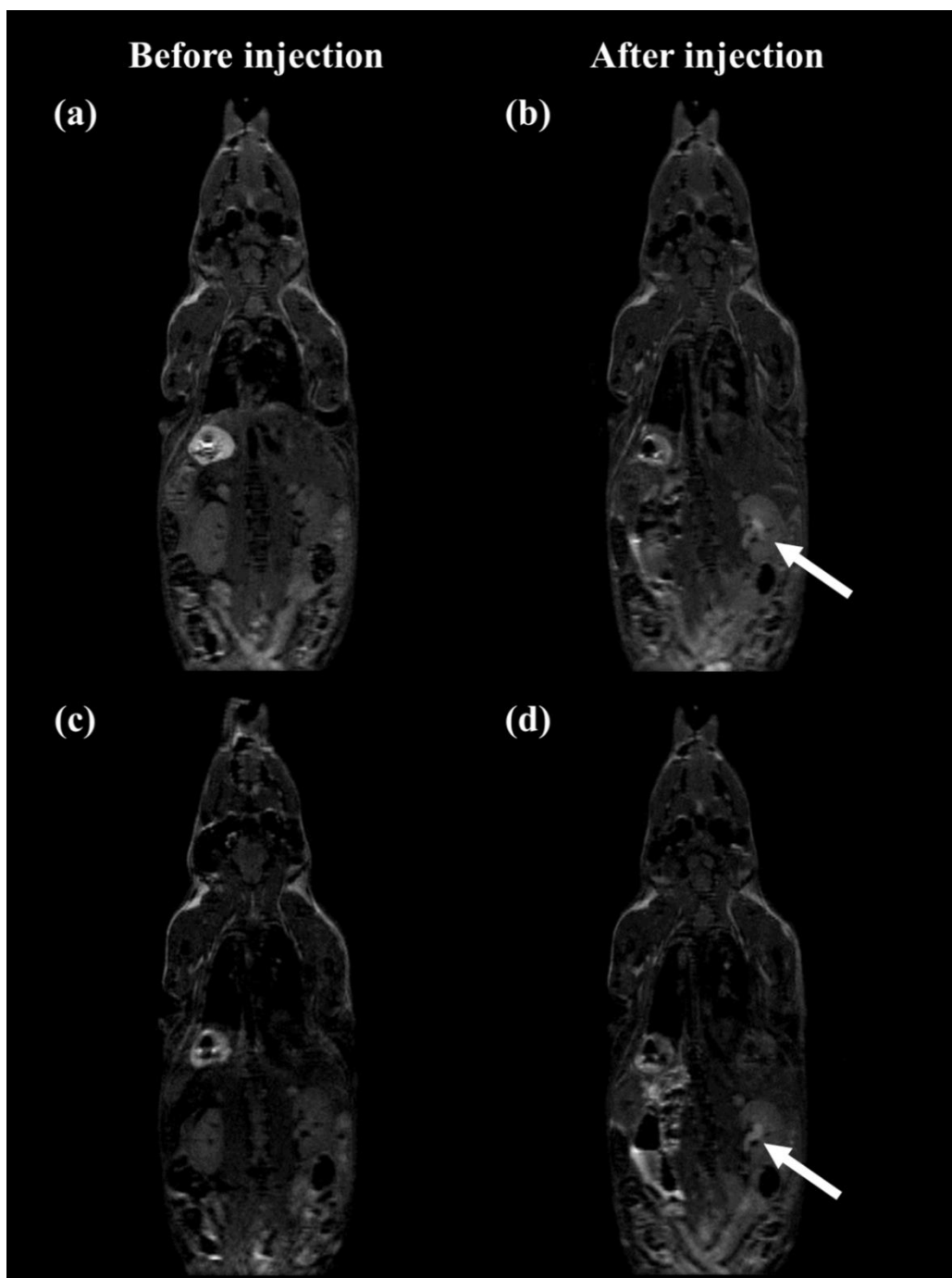


**Figure S6.** *In vivo* MRI coronal images of a mouse (a, c) before injection and (b, d) after intraperitoneal injection of CQDs co-doped with N, Gd and Yb. Arrows point the contrast-enhanced regions observed at an early time after injection (~ 30 min).